Analysis of the Flow in Stalling Engine Inlet Models with Different Visualization and Measurement Techniques

S. Schulze* and C.J. Kähler†

University of the German Armed Forces Munich, 85577 Neubiberg, Germany

Abstract

In this paper the turbulent separation bubble in a jet engine inlet at take-off conditions is investigated in a low-speed wind tunnel. A flow-through nacelle with a boundary layer loading similar to powered engines is used as a wind tunnel model, and the onset, size and topology of the separation bubble is analyzed with oil flow pictures, static pressure measurements and stereoscopic PIV measurements. Sensitivities of the flow in the inlet to the way transition is introduced and to small changes in the experimental setup are explained.

Nomenclature

U_∞	Onstream velocity	[m/s]
c	Chord length	[m]
c_p	Pressure coefficient	[ ]
u	Blow-out velocity at the orifices	[m/s]
x	Variable of the cartesian coordinate system	[m]
z	Variable of the cartesian coordinate system	[m]
α	Angle of attack	[°]
AWM	Atmosphärischer Windkanal München	
$DEHS$	Di-ethylhexyl sebacate	
DFG	Deutsche Forschungsgemeinschaft	
PIV	Particle Image Velocimetry	
PSP	Pressure Sensitive Paint	
$SPIV$	Stereo Particle Image Velocimetry	

---

*Research Scientist.

†Professor.

1   Introduction

Separations in the inlet of a jet engine represent the limit of safe flight conditions. Large-scale structures in the separated flow are usually unsteady and feature a vortex shedding which can cause an inhomogeneous onstream to the fan stage. The resulting fluctuations in mass flow and pressure distribution can give rise to separations at the subsequent compressor stages and also to strong dynamic loadings on the blades which in turn might cause the engine to run unstable. In order to ensure flight safety at the limits of the flight envelope big safety margins are applied for modern transport aircrafts. The performance of a jet engine and the flight envelope can be used to a better capacity if one is able to numerically predict the onset, size and topology of the unsteady structures in the separated flow in a reliable way. While numerical simulation methods for the flight design point are well developed, the simulation of powered engines at the limit of the flight envelope still needs major improvement. The development of such a sophisticated simulation methodology is the objective of the DFG (Deutsche Forschungsgemeinschaft) funded research group FOR1066.

In order to enable the improvement of simulation methodologies, well-designed wind tunnel experiments are essential because thus a high-quality data base can be established for validation purposes. In the past the separation behaviour of jet engine inlets was investigated with common probe measurement techniques which is referred to in the proceedings of different symposia (cf. [1], [2]). Further investigations about the influence of the inlet geometry on the separation behaviour can be found in the literature about inlet design in [3] and also in [4]. In more recent research the inlets of transport aircrafts were analysed with pitot tubes which featured partially time-resolved measurement techniques (cf. [5]). Thus conclusions to the unsteady flow field are confined and it can be stated that no systematic results regarding the unsteady flow structures in the inlets of transport aircrafts are known which are sufficient for the planned validation of the improved simulation methodology. A systematic analysis of the unsteady vortex shedding in the inlet with time-resolving measurement techniques is therefore the objective of this project. Taking advantage of recent progress in the field of Particle Image Velocimetry the unsteady structures in the separated flow can be identified and characterized without the disturbing influence of a probe. The works of [6], [7], and [8] show that a detailed flow analysis with the stereoscopic, tomographic, and time-resolved PIV measurement techniques is possible.

2   Experimental Setup

The basic wind tunnel experiments are conducted in a low-speed wind tunnel of the Eiffel type (Atmosphärischer Windkanal München, AWM) which has a test section of $1.85m \times 1.85m$. The wind tunnel model is an axisymmetric flow-through nacelle which is attached to the floor of the test section by a traverse for changes in the angle of attack (see Fig. 1). Because of the high costs for an air venting device the fundamental wind tunnel experiments arrange for a flow-through nacelle and not for a real jet engine with an integrated fan and a realistic mass flow rate. In order to be able to investigate the characteristic separation behaviour of a jet engine, a flow-through nacelle was designed which mimics the boundary layer loading of a real engine at take-off conditions. The design methodology which was used for this objective and the numerical investigations for a realistic reference jet engine are described in [9].

The axisymmetric wind tunnel model has a length of $526mm$ and a leading edge diameter of $315mm$ according to the investigated reference nacelle called LARA (cf. [10]). Related to the chord length of the flow-through nacelle a Reynolds number of 1.3×10^6 is achieved at an onstream velocity of $38m/s$. A good optical accessibility for the planned PIV measurements is ensured by employing Plexiglas as a material in the middle segment of the nacelle. An aerodynamic casing in the shape of a NACA 0033 airfoil underneath the nacelle and a thoroughly designed outer contour of the nacelle guarantee that the flow inside of the nacelle is unaffected by possible separations on the outside.
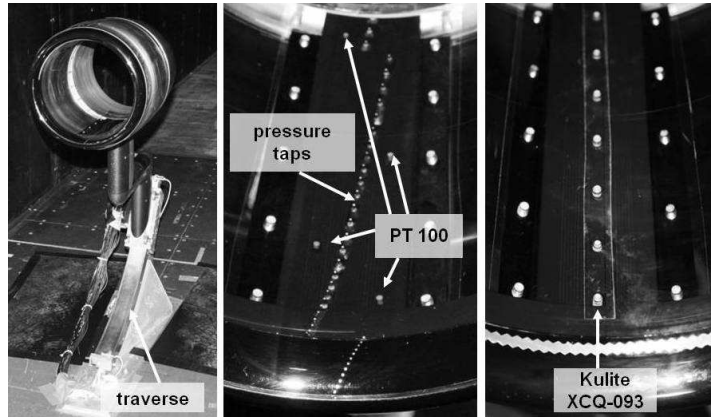
Figure 1: Wind tunnel model (left) with static pressure taps (middle), and pressure transducers for unsteady pressure measurements (right).

The wind tunnel model features 48 static pressure taps with a diameter of $0.3mm$ from about 5% chord length on the outside of the nacelle to about 60% chord length in the inlet (see Fig. 1). The staggered alignment of the pressure taps over a circumferential section of $\pm5°$ ensures that the taps do not disturb one another. In the numerical simulations the resulting pressure distribution hardly differs from the pressure distribution in the straight bottom section of the nacelle (not shown here). Figure 1 also depicts the mounting positions for four PT 100 temperature sensors which are needed for Pressure Sensitive Paint and Infrared measurements.

The rotational symmetry and the possibility to mount the Plexiglas part of the nacelle in arbitrary positions on the aft part permit for the integration of various measurement equipment in the same wind tunnel model. Thus seven pressure transducers of the type Kulite XCQ-093 are placed flat to the surface in another circumferential section of the nacelle in a way that they can measure a differential pressure of $\pm350mbar$ with a limiting frequency of up to $11kHz$.

3   Transition

The application of transition strips on a curved surface like the one that the flow-through nacelle features is not easy to handle because the strip cannot be fixed in the same place more than once. Since the flow within the inlet can be influenced by the way transition is introduced, special emphasis was put on reproducibility during the design process. It was planned to introduce transition by blowing out normal to the wall through 160 orifices close to the leading edge between the stagnation point and the suction peak ($x/c = 0.004$). The orifices have a diameter of $0.4mm$ and are distributed in a circumferential distance of 2.25% according to the investigations of Horstmann et al. [11]. Every eight orifices are connected to one settling chamber which again is supplied with pressurized air (cf. Fig. 2).

In order to introduce transition in a reproducible way one has to be able to adjust a specific blow-out ratio u/U_∞ of the velocity at the orifices to the onstream velocity. During the experiments a defined mass flow rate through the orifices was accomplished with the help of a flow meter ($0.02m^3/h$ to $0.2m^3/h$) and a pressure reducer of 1 bar. Consistent flow rates were guaranteed by a 190,000 l reservoir of compressed air at 20 bar which was not in use elsewhere during the time of the experiments.

The objective of the transition investigations was to determine a blow-out ratio which is sufficient to trip the flow but at the same time small enough to avoid an overtripping. If the blow-out ratio is chosen too big, separation onset will occur at smaller angles of attack and the turbulent separated regions at higher angles of attack will appear too large. This effect can be seen in Fig. 3 which shows a comparison of the pressure distributions in the bottom section of the flow-through nacelle at an angle of attack of 23° for different blow-out ratios. Apparently the static pressure distributions resemble a flow without a laminar leading edge separation and without an overtripping the better the smaller the blow-out ratio becomes. The boundary layer at 0.4% chord length is assumed to be so thin that only very small blow-out velocities need to be applied. In this case even the irregularities in the surface finish from drilling the orifices seem to be sufficient to trip the flow. Note that with a completely smooth surface without blowing orifices laminar leading edge stall occurs at much smaller angles of attack (not shown here).

Thus it was decided to continue the experiments without blowing out in order to avoid an overtripping. The above investigations were undertaken for equivalent blow-out velocities at all orifices. The initial idea was that a variation of the blow-out amplitude over the circumference of the nacelle might be favourable. However, oil film pictures

Figure 2: Position of the blow-out orifices in the wind tunnel model.

Figure 3: Influence of the blow-out ratio on the pressure distributions, $alpha = 23°$, $Re = 1.3 \times 10^6$.

showed that the inlet flow could be easily disturbed in its symmetry to the xz-plane if staggered blow-out amplitudes were used. This is probably due to small inaccuracies in the manufacturing process of the orifices and the nacelle's contour. Evenly spread blow-out amplitudes on the other hand always resulted in symmetric flow fields which is why this way of introducing transition was investigated in detail.
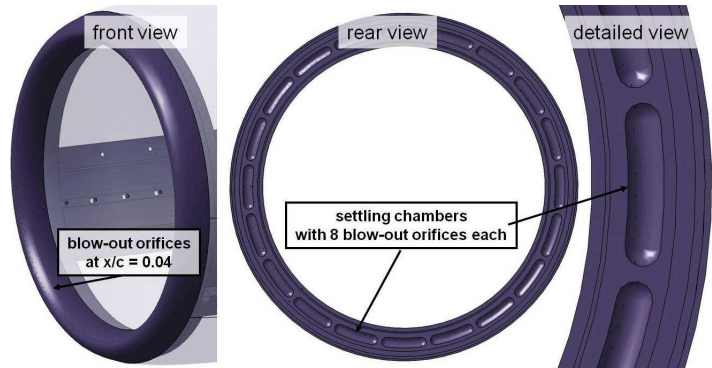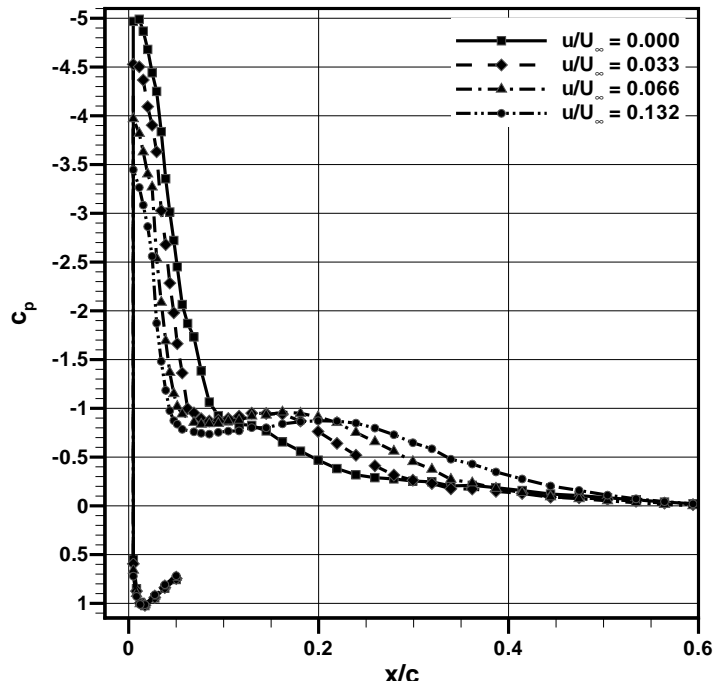
4 Sensitivities of the Separated Flow

In the following section the sensitivities of the separated flow to the way transition is introduced and to small changes in the experimental setup is investigated. Consolidated findings referring to the influences on the inlet flow are important for validation purposes.

4.1 Influence of the Tripping Method

Figures 4 to 8 show oil flow pictures for a range in angle of attack between $\alpha = 5°$ and $\alpha = 25°$. The flow again is tripped by the roughness of the drilled blow-out orifices $(u/U_\infty = 0)$ at $x/c = 0.004$. In Figure 4 a small laminar separation bubble close to the leading edge can be observed which is followed by an adjacent, turbulent flow further downstream. At higher angles of attack, on the other hand, a turbulent separation bubble evolves downstream of the laminar separation bubble which is characteristic for the separation behaviour of a jet engine inlet (cf. Fig. 5 to 8). As expected the size of the turbulent separation bubble grows with increasing angle of attack in the axial and circumferential direction. The laminar separation bubble, however, does not behave as expected. A closer look at the laminar separation bubble in Fig. 9 for an angle of attack of 23° reveals that the bubble is no longer intact in its shape for higher angles of attack. In fact, small indents occur at even distances to each other which cannot be observed at small angles of attack. The distance between the indents is equal to the length of one settling chamber which is connected to eight blow-out orifices each (cf. 2). At high angles of attack the pressure difference between the ends of the settling chamber obviously causes the flow to circulate within the settling chamber. Thus air is blown out towards the middle of the nacelle and sucked in toward the outside of the nacelle. This results in a saw-tooth like blow-out distribution over the circumference of the nacelle even though no pressurized air is applied to the settling chambers at all.

In order to determine to what degree the size and topology of the turbulent separation bubble is affected by this saw-tooth like blow-out distribution, transition strips were additionally investigated as a common tripping method. Regarding transition strips with a thickness of less than $50\mu m$, it was impossible to apply the strips to the curved surface of the nacelle in a persistent way. Every attempt resulted in an asymmetric flow field because the flow close to the leading edge is sensitive to the smallest kinks in the transition strip. Transition strips with a height above $50\mu m$ on the other hand showed a definite overtripping. The transition strip with a thickness of $50\mu m$ was therefore chosen and fixed right on top of the blow-out orifices.
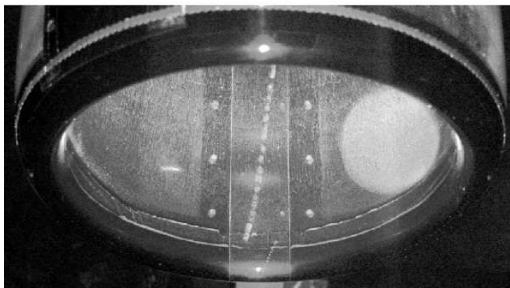

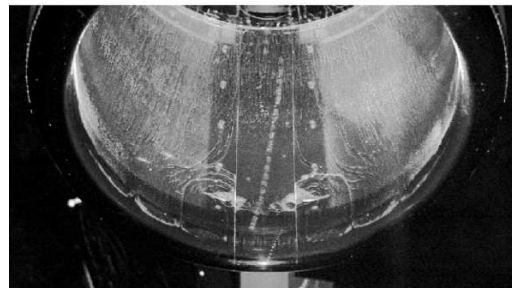Figure 4: Oil flow picture, $u/U_\infty = 0$, $\alpha = 5°$, $Re = 1.3 \times 10^6$.

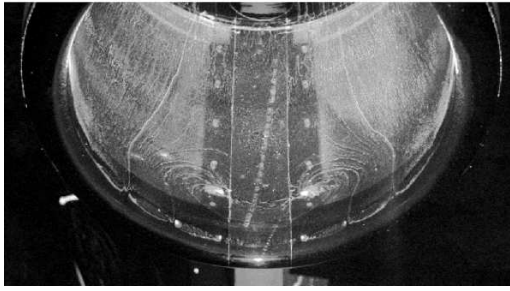Figure 5: Oil flow picture, $u/U_\infty = 0$, $\alpha = 22°$, $Re = 1.3 \times 10^6$.

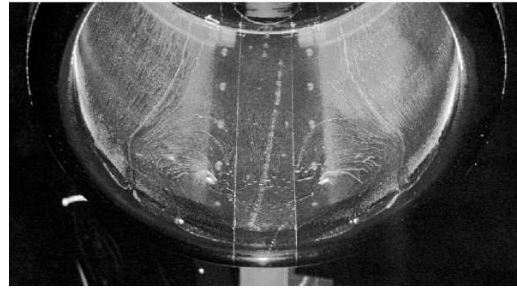Figure 6: Oil flow picture, $u/U_\infty = 0$, $\alpha = 23°$, $Re = 1.3 \times 10^6$.

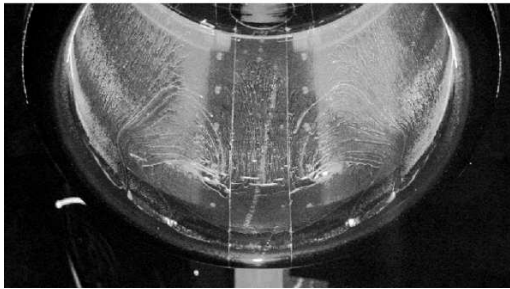Figure 7: Oil flow picture, $u/U_\infty = 0$, $\alpha = 24°$, $Re = 1.3 \times 10^6$.

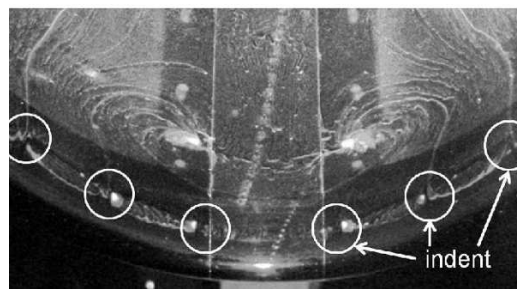Figure 8: Oil flow picture, $u/U_\infty = 0$, $\alpha = 25°$, $Re = 1.3 \times 10^6$.

Figure 9: Indents in the laminar separation bubble, $\alpha = 23°$.

The Figures 10 to 15 show the oil flow pictures for the chosen, 2 mm wide transition strip. At small angles of attack the oil flow pictures for both tripping methods hardly differ at all. Again a laminar separation bubble with an adjacent, turbulent flow further downstream can be observed (see Fig. 10). At angles of attack well above 22° the characteristic turbulent separation bubble evolves also for a tripping with the transition strip (cf. 11 to 15). The only difference between the two tripping methods is the angle of attack where separation onset occurs. From the oil flow pictures it cannot precisely be stated when separation onset takes place but it seems that the tripping case with the transition strip tends to separate at higher angles of attack than the tripping case with $u/U_\infty = 0$.

A comparison of the pressure distributions for both tripping methods confirms that the separation onset for $u/U_\infty = 0$ occurs one degree earlier in angle of attack than for the transition strip, namely at $\alpha = 23°$ and $\alpha = 24°$ (cf. Fig. 16). Another difference between the two tripping method is their hysteresis behaviour. While the tripping method with $u/U_\infty = 0$ clearly features hysteresis, the tripping method with the transition strip is not or hardly at all affected by hysteresis. The Figures 17 and 18 show a comparison of the pressure distributions for the case that the final angle of attack is advanced from smaller angles of attack and from bigger angles of attack, respectively.

4.2   Influence of the Experimental Setup

If the pressure distributions for the tripping case $u/U_\infty = 0$ in Fig. 16 are compared to the according oil flow picture for $\alpha = 22°$ (cf. Fig. 5, one can see that they are not in agreement regarding the separation onset. While the oil flow picture already depicts a turbulent separation
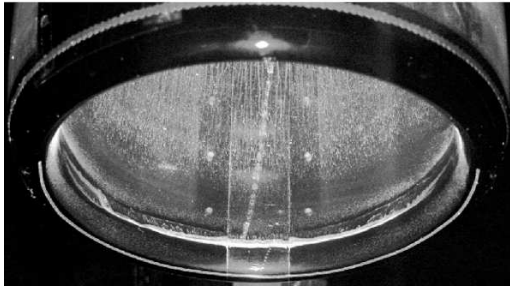
Figure 10: Oil flow picture, $50\mu m$ strip, $\alpha = 5°$, $Re = 1.3 \times 10^6$.
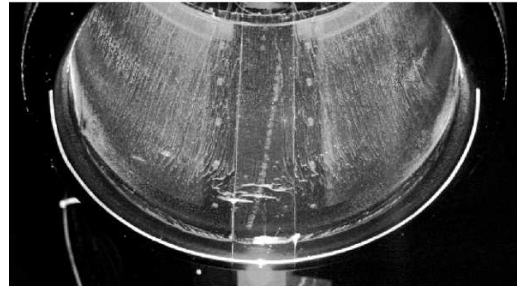

Figure 11: Oil flow picture, $50\mu m$ strip, $\alpha = 22°$, $Re = 1.3 \times 10^6$.
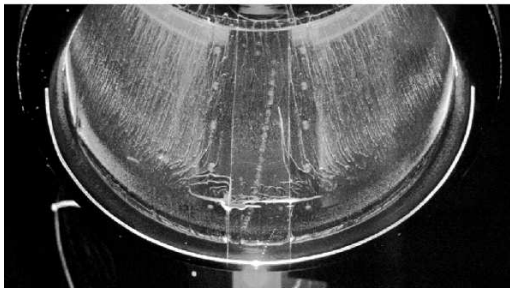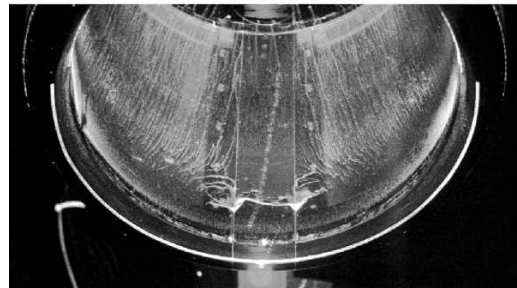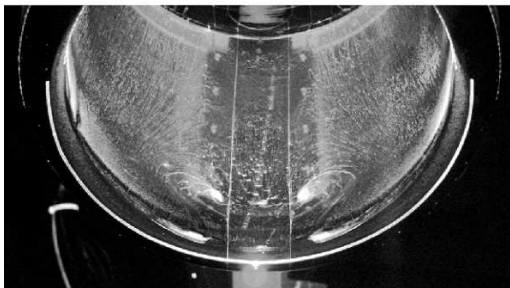

Figure 12: Oil flow picture, $50\mu m$ strip, $\alpha = 23°$, $Re = 1.3 \times 10^6$.

Figure 13: Oil flow picture, $50\mu m$ strip, $\alpha = 24°$, $Re = 1.3 \times 10^6$.

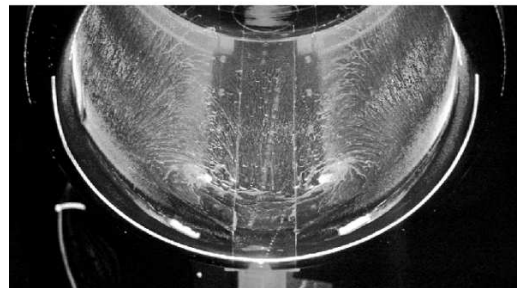Figure 14: Oil flow picture, $50\mu m$ strip, $\alpha = 25°$, $Re = 1.3 \times 10^6$.

Figure 15: Oil flow picture, $50\mu m$ strip, $\alpha = 26°$, $Re = 1.3 \times 10^6$.

bubble at $\alpha = 22°$, the pressure distribution shows an adjacent flow. The reason for this difference is a tape in the middle of the flow-through nacelle which was used in order to cover the static pressure taps during the making of the oil flow pictures. Static pressure measurements with a punctured tape at the positions of the pressure taps resulted in pressure distributions which feature an earlier separation onset than the measurements without the tape in the middle of the nacelle for both tripping methods (cf. Fig. 19 and 20). In fact separation occurred one degree earlier, namely at $\alpha = 22°$ for the tripping case with $u/U_\infty = 0$ and at $\alpha = 23°$ for the tripping case with the transition strip.

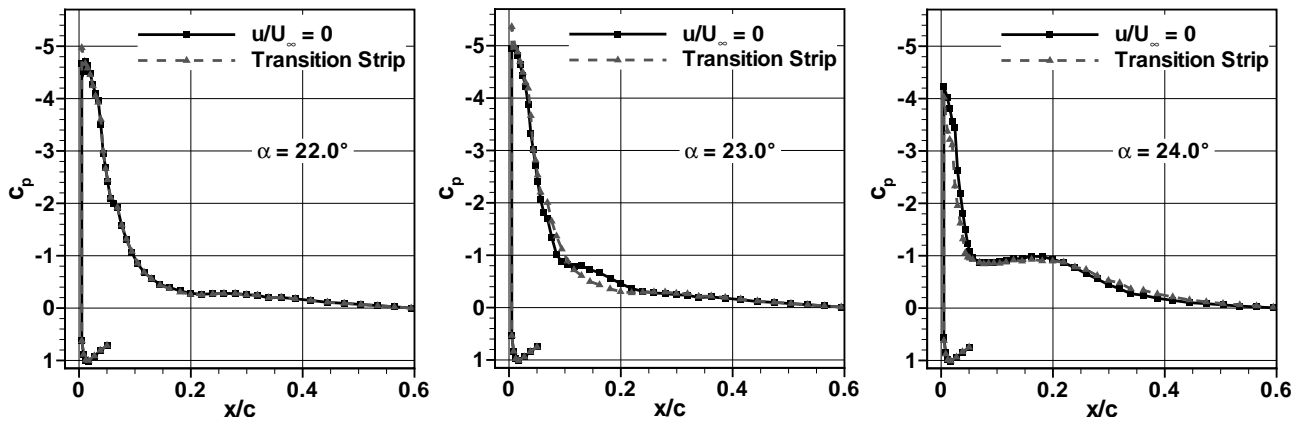Figure 16: Comparison of the pressure distributions for both tripping methods, $alpha = 22°$ to $24°$, $Re = 1.3 \times 10^6$.
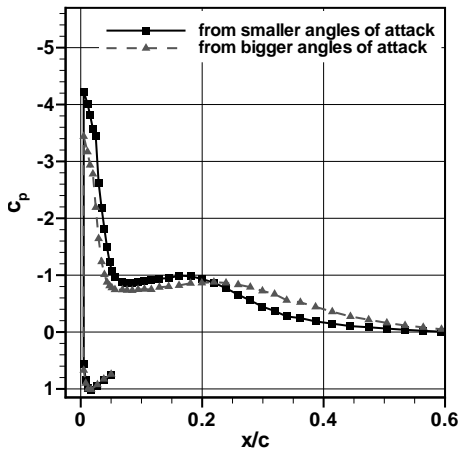

Figure 17: Hysteresis investigation, $u/U_\infty = 0$, $\alpha = 24°$, $Re = 1.3 \times 10^6$.
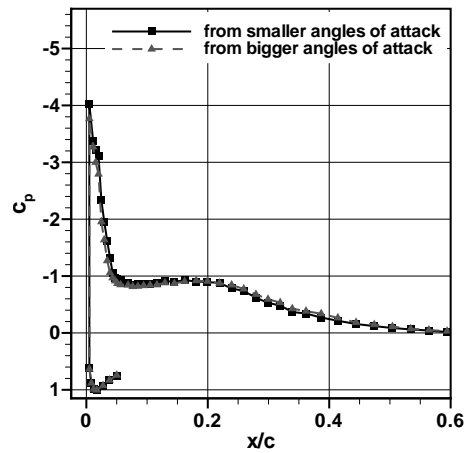

Figure 18: Hysteresis investigation, $50\mu m$ strip, $\alpha = 24°$, $Re = 1.3 \times 10^6$.
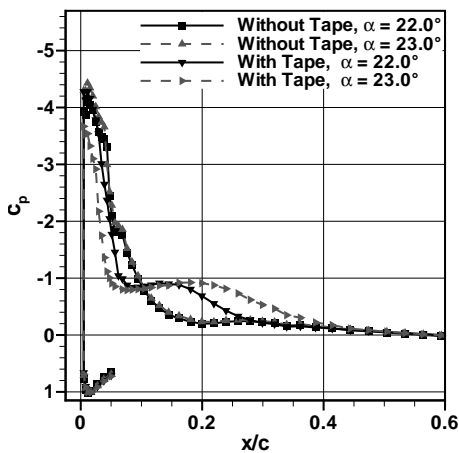

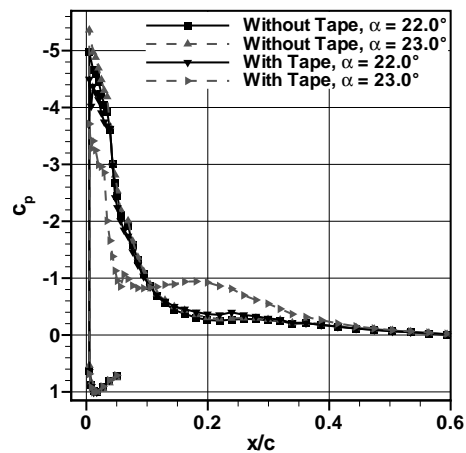Figure 19: Tape influence, $u/U_\infty = 0$, $\alpha = 22°$ and $23°$, $Re = 1.3 \times 10^6$.

Figure 20: Tape influence, $50\mu m$ strip, $\alpha = 22°$ and $23°$, $Re = 1.3 \times 10^6$.

5 Stereo Particle Image Velocimetry

So far the size of the turbulent separation bubble in axial and circumferential direction has been analyzed. Stereoscopic PIV measurements were conducted to determine the height of the turbulent separation bubble. The experimental setup therefore featured a Nd:YAG double pulse laser with a pulse energy of $2 \times 400mJ$, two PCO 4000 CCD cameras, and as well the according Scheimpflug adapters, 2x teleconverters, and two objective lenses with a focal length of $100mm$. The field of observation is located in the vertical symmetry plane of the flow-through nacelle and is parallel to the direction of the onstream velocity. The CCD cameras are mounted on top of the wind tunnel and are aligned in a $39°$ angle to the field of observation each. A redirecting mirror behind the wind tunnel model makes it possible to measure in a beneficial forward scattering setup. The seeding particles have a size of about $1\mu m$ and are composed of DEHS (di-ethylhexyl sebacate). The light sheet optics are placed outside of the wind tunnel, and a 2D calibration plate which could be shifted with the help of a micrometer bench was used for calibration purposes.

For the analysis of the vector fields 200 instantaneous vector fields were averaged at a time. Again the influence of both tripping methods and the covering tape in the middle of the nacelle were investigated for angles of attack between $22°$ and $25°$. In all cases no turbulent separation bubble could be observed in the averaged vector fields for $\alpha = 22°$ and $\alpha = 23°$. Figure 21 exemplifies such an averaged vector field with an assumed, adjacent flow for the tripping case with $u/U_\infty = 0$ and the covering tape attached. The vector length hereby is related to the overall velocity within the flow field while the colour depicts the axial component of the velocity vector. In front of the nacelle the chosen onstream velocity of $38m/s$ could be measured, and in the vicinity of the suction peak a rise in the axial component of the velocity can be seen as expected. A turbulent separation bubble as it was observed in the according pressure distribution, however, cannot be found.

In the figures 22 to 26 the cases which feature a turbulent separation bubble in the averaged vector field are shown, and it can be seen that the separation bubble for both tripping cases with the covering tape attached grows if the angle of attack is changed from $24°$ to $25°$. The investigated case with the covering tape attached and the tripping method $u/U_\infty = 0$ even displays a leading edge stall at $\alpha = 25°$ (cf. Fig. 24) while the cases without the covering tape solely illustrate a separation for $u/U_\infty = 0$ at $\alpha = 25°$ (cf. Fig. 26). Thus the results from the SPIV measurement are not in good agreement with the static pressure measurements. However, if one analyzes the instantaneous vector fields, it can be observed that all cases that indicate a turbulent separation bubble according to the measured pressure distributions feature a vortex shedding. Thus it can be concluded that the height of the separation bubble in all of these cases has to be smaller than $4mm$ which is about the region above the nacelle surface that cannot be resolved. On the one hand reflections at the static pressure taps had to be cut out of the particle images which goes along with a loss of information. On the other hand the field of observation is quite big which limits the capability of a good resolution. A better resolution of the turbulent separation bubble can be achieved if the $100mm$ objective lenses are changed for lenses with a bigger focal length. The field of observation thus becomes smaller and the reproduction scale more favourable. Reflections at the surface can be avoided if a circumferential section of the nacelle without any probes or taps is used during the measurements.
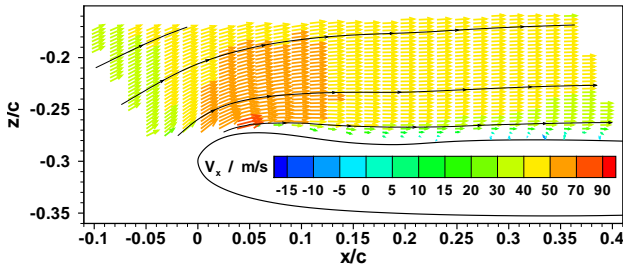
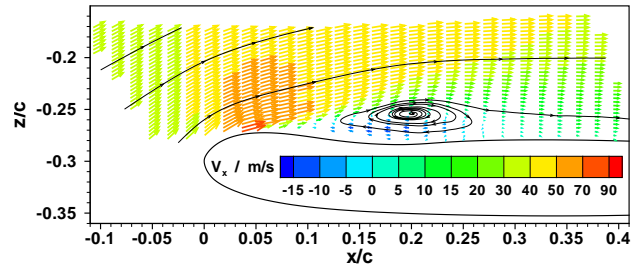Figure 21: Vector field, $u/U_\infty = 0$, with tape, $\alpha = 22°$, $Re = 1.3 \times 10^6$.

Figure 22: Vector field, $u/U_\infty = 0$, with tape, $\alpha = 24°$, $Re = 1.3 \times 10^6$.
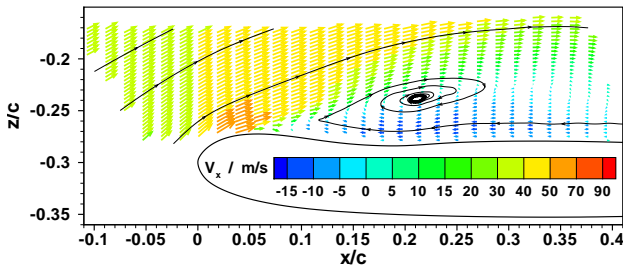

Figure 23: Vector field, $50\mu m$ strip, with tape, $\alpha = 24°$, $Re = 1.3 \times 10^6$.

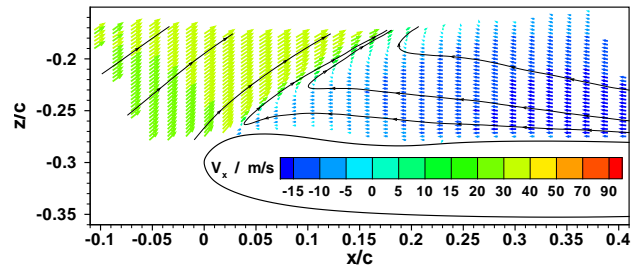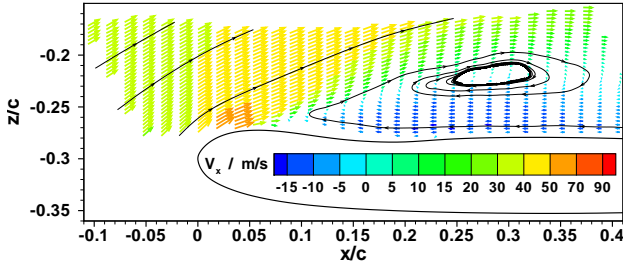Figure 24: Vector field, $u/U_\infty = 0$, with tape, $\alpha = 25°$, $Re = 1.3 \times 10^6$.

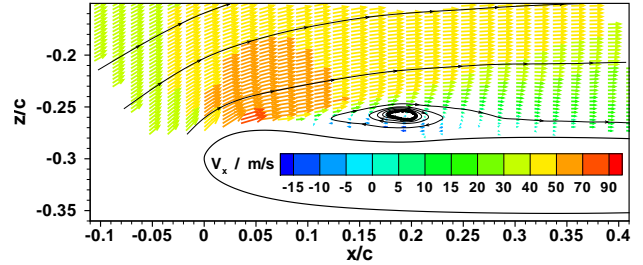Figure 25: Vector field, $50\mu m$ strip, with tape, $\alpha = 25°$, $Re = 1.3 \times 10^6$.

Figure 26: Vector field, $u/U_\infty = 0$, without tape, $\alpha = 25°$, $Re = 1.3 \times 10^6$.

6 Conclusion and Outlook

Based on the results of the first measurement campaign it can be stated that it was possible to design a flow-through nacelle which mimics the boundary layer loading of a jet engine at take-off conditions. The onset and size of the characteristic turbulent separation bubble was found to be sensitive to the way transition is introcuced and also to small changes in the experimental setup like a thin tape attached to the nacelle's surface. In fact separation onset shifts to different angles of attack between $\alpha = 22°$ and $\alpha = 24°$ for the investigated setup cases which is an important piece of information for the planned validation of the new simulation methodology. According to SPIV measurements the height of the separation bubble is in the majority of the cases smaller than $4mm$ for different tripping methods unless the experimental setup is changed by a tape in the middle of the nacelle.

During the next measurement campaign the SPIV measurements are meant to be repeated with a better resolution of the nearby region of the nacelle's surface. Thus the exact height of the turbulent separation bubble will be determined in an observation plane parallel and perpendicular to the onstream direction. The SPIV measurements will be complemented by tomographic and rime-resolving PIV measurements giving information about the instantaneous flow fields in 3D and the dynamics of the unsteady structures in the separated flow, respectively. Extensive information about the static pressure distributions in the inlet and also on the outside of the nacelle will be gained with Pressure Sensitive Paint measurements. Characteristic frequencies of the vortex shedding will be investigated with special pressure transducers and hot-wire anemometry. Infrared measurements will round off the analysis of the inlet flow.

Acknowledgments

References

[1] Rekos et al.: "Inlets and Nozzles for Aerospace Engines", AGARD, CP No. 91, 1971.

[2] Dini et al.: "Engine Response to Distorted Inflow Conditions", AGARD, CP No. 400, 1986.

[3] Goldsmith, E.L., Seddon, J.: "Practical Intake Aerodynamic Design", AIAA Education Series, Second Edition, 1999.

[4] Willmer, A.C., Brown, T.W., Goldsmith, E.L.: "Effects of Intake Geometry on Circular Pitot Intake Performance at Zero and Low Forward Speeds", AGARD, CP No. 301, 1981.

[5] Quémard, C., Garçon, F., Raynal, J.-C.: "High Reynolds Number Air Intake Tests in ONERA F1 and S1Ma Wind-Tunnels", In: H. Hoheisel (Ed.): "Aspects of Engine-Airframe Integration for Transport Aircraft", Proceedings of DLR Workshop, DLR Mitt. 96-01, 1996.

[6] Elsinga, G., Scarano, F., Wieneke, B., Oudheusden, B.: "Tomographic Particle Image Veloci-metry", Exp. Fluids 41, pp. 933-947, 2006.

[7] Hain, R., Kähler, C.J., Michaelis, D.: "Tomographic and Time Resolved PIV Measurements on a Finite Cylinder Mounted on a Flat Plate", 7th International Symposium on Particle Image Velocimetry, Rom, Italy, September 11-14, 2007.

[8] Hain, R., Kähler, C.J., Radespiel, R.: "Dynamics of Laminar Separation Bubbles at Low-Reynolds-Number Aerofoils", Journal of Fluid Mechanics, Vol. 630, pp. 129-153, July 2009.

[9] Schulze, S., Kähler, C., Radespiel, R.: "On the Comparison of Stalling Flow-Through Nacelles and Powered Inlets at Take-Off Conditions", First CEAS European Air and Space Conference, Berlin, Germany, September 10-13, 2007.

[10] Mullender, A.J., Lecordix, J.L., Lecossais, E., Godard, J.L., Hepperle, M.: "Hybrid Laminar Flow Nacelle Design", 20th Congress of the International Council of the Aeronautical Sciences, Sorrento, Napoli, Italy, September 8-13, 1996.

[11] Horstmann, K.H., Quast, A.: "Widerstandsverminderung durch Blasturbulatoren", DLR Forschungsbericht FB 81-33, 1981.